Preprint of paper published in Combustion and Flame, 232:111499, 2021.
https://doi.org/10.1016/j.combustflame.2021.111499

Thermal Ignition by Vertical Cylinders

Silken Jones, Joseph Shepherd

California Institute of Technology,
1200 E. California Blvd., Pasadena, California, 91125, United States

Abstract

In this work, thermal ignition of laminar external natural convection flows by vertical cylinders is investigated. Effects of cylinder size are studied, with cylinder height ranging from 12.7 to 25.4 cm, and cylinder surface areas varying from 25 to 200 cm^2. The minimum ignition threshold for a stoichiometric hexane-air mixture is 1019 K for a cylinder 25.4 cm long and 200 cm^2 in surface area. The ignition threshold is found to have a weak dependence on surface area, in contrast to historical data. The ignition results are consistent with ignition temperature decreasing inversely with the logarithm of surface height. Experiments are performed with multi-component, heavy-hydrocarbon fuels including POSF-4658 Jet A and two surrogate fuels, Aachen and JI, as well as hexane. The setup is heated for multi-component fuel testing. POSF-4658 Jet A has an ignition temperature of 971 K at an ambient temperature of 333 K. All fuels investigated were found to have ignition thresholds within 38 K of the POSF-4658 Jet A ignition threshold. JI is found to be the most appropriate surrogate for POSF-4658 Jet A.

Keywords: thermal ignition, natural convection, safety

1. Introduction

Accidental thermal ignition events pose a serious safety hazard to industrial processes. It is important to understand how the conditions of the hot surface, such as flow configuration, surface orientation, and surface geometry, influence the thermal ignition behavior. Current safety standards do not account for such changes in hot surface conditions. For example, the current Federal Aviation

Email address: smjones@caltech.edu (Silken Jones)

Administration (FAA) regulations limit the maximum allowable temperature in a flammable leakage zone of an aircraft to 477 K [1]. This regulation does not consider the hot surface size, flow regime, or geometry of the region surrounding the surface.

Past studies of thermal ignition by internal natural convection flows include the work of Kuchta et al. [2], White [3], Boettcher [4], and Martin and Shepherd [5]. These studies deal with surfaces greater than 40 cm^2 in area. Available literature data on thermal ignition by external natural convection flows, by contrast, predominantly examines thermal sources with much smaller surface areas. The works of Adomeit [6], Ono et al. [7], Melguizo-Gavilanes et al. [8], and Boeck et al. [9] study surfaces less than 10 cm^2 in area.

In this work, the ignition behavior of external natural convection flows is investigated by using a vertical cylinder as a thermal ignition source. The surface area of the ignition source ranges from 25 to 200 cm^2 in an effort to expand the range of data available for thermal ignition of external natural convection flows to surface areas comparable to existing data on internal natural convection ignition events. We examine the influence of geometrical parameters like surface area and vertical dimension (height) in addition to flow configuration in our study of ignition of n-hexane fuel mixtures. We also measure thermal ignition thresholds for complex fuels like aviation kerosene and multicompent kerosene surrogates. There are extensive studies of Jet A and surrogates focused on high temperature and pressure combustion and the present study on hot surface ignition behavior is designed to complement those studies by providing data on ignition of these fuels in the low pressure and low to intermediate temperature regime. The goal is to identify appropriate surrogates for Jet A for further hot surface ignition testing.

2. Experimental Methods

The surfaces studied are vertical cylinders constructed from stainless steel tubing. The wall thickness of all the cylinders investigated is 0.05 cm. The height of the cylinders range from 12.7 cm to 25.4 cm, and the surface areas of the tested cylinders varies from 25 to 200 cm^2. The geometry of the cylinders is reported in Table 1. The following sections describe the experimental apparatus, characterization of the heated surface, and key optical diagnostic techniques.

Label	Surface Area (cm^2)	Height (cm)	Diameter (cm)
25A	25	25.4	0.31
50A	50	25.4	0.64
50C	50	12.7	1.27
75B	75	19.1	1.27
100A	100	25.4	1.27
100C	100	12.7	2.54
200A	100	25.4	2.54

Table 1: Geometry of tested cylinders.

The experiments are conducted inside a 40 L cylindrical combustion vessel with a 30.4 cm diameter and a height of 66.0 cm. A cylinder is held in place inside the combustion vessel with a copper support structure as shown in Figure 1. The support structure provides a path for current flow, as the cylinder is resistively heated. The ends of the cylinder are water cooled in order to force a constant temperature of 298 K in the support structure. This prevents the support structure from heating up during testing due to conduction from the heated cylinder.

When preparing an ignition experiment, the combustion vessel is filled with a flammable mixture. The vessel is first evacuated and then a syringe is used to inject liquid fuels into the evacuated vessel. Nitrogen and oxygen gases are added to make the desired fuel-air mixture at an initial pressure of 101.3 KPa. A manometer (MKS model 121A-01000B) with an accuracy of 0.01 kPa is used to monitor the pressure during filling, as the method of partial pressures is used to control mixture composition. After the vessel is filled, a fan mixer is turned on for three minutes to ensure a homogeneous fuel-air mixture, and then turned off and the gases allowed to settle for another three minutes to ensure a quiescient mixture at the start of each test.

Up to 600 A is applied to the resistive heating circuit using a remotely controlled Manga Power XR5-600 power supply. The output of the power supply is controlled via a LabView script in order to heat the cylinder to a set temperature, and it takes the cylinders approximately 20 to 60 s to reach steady state depending on the mass (see Figure 2 of the Supplementary Materials.) A two-color pyrometer monitors the surface temperature as described in Section 2.1.1 and is used to provide feedback control. A natural convection flow develops over the exterior of the cylinder surface during the heating process and the interferometer is used

to make quantitative measurements of the gas surrounding the hot cylinder. The maximum test time is limited to 300 s. This limitation and the volume of the combustion vessel ensures that no recirculation of gas through the heated boundary layer occurs. If an ignition event has not occurred at the end of the test duration, the experiment is stopped and is considered as a non-ignition result.

Experiments with heavier multicomponent fuels require heating of the entire experimental setup. A multi-zone heating system is installed, with a total available power of 10.8 kW. Each zone has a number of flexible silicone-rubber heaters from Omega and a type E thermocouple for temperature monitoring. Closed-loop control of temperature is achieved with Watlow 935A PID controllers. Further details are given in the Supplementary Materials.

2.1. Diagnostics

Several diagnostics are used in the experiments. Non-contact surface temperature measurements of the cylinder are made via a two-color pyrometer. Type K thermocouples are spot welded to the cylinder surface and provide a secondary measurement of surface temperature. A Mach-Zhender interferometer takes quantitative measurements of the temperature field of the gas surrounding the cylinder. A piezoresistive pressure transducer provides transient pressure measurements and is used to verify the occurrence of an ignition event.

2.1.1. Surface Temperature Diagnostics

Non-contact measurements of surface temperature are made by a two-color pyrometer [10]. The ratio of intensities of two different wavelengths of light, I_1/I_2, is used to determine the surface temperature T_S:

$$T_S = \frac{A}{\ln(\frac{I_1}{I_2}) - B} \tag{1}$$

Calibration with a blackbody radiation source (Process Sensors BBS1200) determines constants A and B.

Initial characterization of the cylinders shows that the central portion of a cylinder reaches a uniform temperature. Approximately the last two centimeters at each end of a cylinder are cooler due to conduction to the water cooled ends. To test

the pyrometer operation immediately before ignition testing, pyrometer measurements of the central hot region of the cylinder are checked against thermocouple measurements taken in the same region. Additionally, a thermocouple is spot welded at the top of the cylinder in the cooler region at the edge. This is above the location where ignition occurs and should not significantly disturb natural convection flow development in the ignition region. The temperature of the central hot region is extrapolated from the temperature reading of the top thermocouple using a correlation developed from preliminary heating tests. The central thermocouple is removed before ignition testing, while the top thermocouple remains to provide a double check for the pyrometer reading. Figure 2 shows a schematic of this situation.

2.1.2. Interferometer

For this work, an interferometer is used to make quantitative temperature field measurements. Merzkirch [11] describes in detail the fundamental principles behind interferometry. Other researchers have used interferometry to study combustion; in particular, Adomeit [6] used a Mach-Zehnder interferometer to measure the development of temperature fields surrounding suddenly heated vertical cylinders over time. The cylinders Adomeit [6] studied are smaller than the ones investigated here (Adomeit's cylinders are 0.3-0.4 cm in diameter and 3.5 cm long, with a surface area of 3.8 cm^2), but the application of interferometry is remarkably similar.

Due to the size of the surfaces studied in this work, the interferometer designed for this investigation needed to have a test beam with a diameter of 100 mm (to match the window aperture). This allows the interferometer to collect the maximum amount of information possible about the gas surrounding the test cylinders, limited only by the size of the windows on the vessel. The interferometer presented here is a variation on a classic Mach-Zehnder interferometer design. In this version, the test beam is expanded to a test section diameter of 101.6 mm, and then condensed before recombining with the reference beam. The reference beam is routed through a single-mode polarization preserving fiber. The new interferometer design is successfully validated against a well-characterized heated surface; this is documented in the Supplementary Materials.

3. Thermal Boundary Layer Measurements

The interferometer described in Section 2.1.2 can be used to inspect the thermal boundary layer in a quantitative manner. The formation of the thermal boundary layer is critical to creating the initial conditions under which ignition occurs, and it is therefore useful to observe the thermal layer directly. Using the exact post-processing procedure described in detail by Coronel et al. [12] based on the fundamental principles presented by Merzkirch [11], the interferometer images can be converted into a radial, two-dimensional field of temperature surrounding the heated surface. Figures 3 and 4 show representative interferometry results from the experiments with hexane. These results come from a 30 s time average of post-processed interferometry temperature fields.

Figure 3 shows the processed temperature fields on the left and right sides of Fig. 3, from an experiment using cylinder 75B in a stoichiometric n-hexane/air mixture, with a surface temperature of 1104 K. The temperature in the gas surrounding the cylinder appears to be uniform within the observation window and is examined in more detail in Fig. 4.

The boundary layer radial temperature profile is sampled from the results shown in Fig. 3 at a height of 12.7 cm from the bottom edge of the cylinder. The boundary layer profiles from the left and right sides of the interferometer images are compared with a prediction of the thermal boundary layer formulated via similarity solution in Fig. 4. A fully variable fluid property formulation of the similarity solution is used, following the procedure laid out by Cairnie and Harrison [13]. Comparison of the left and right boundary layer profiles from interferometry shows they are consistent within 10%, except within 1 mm of the surface, a narrow region known to be prone to larger errors due to the nature of the interferometry post-processing algorithm. The experimental boundary layer profiles are somewhat cooler than the profile predicted by the similarity solution for a wall temperature of 1100 K.

The percent difference between the two experimental boundary layer profiles is less than 10% and the experimental results are reasonably symmetrical. The percent difference between the mean experimental thermal boundary layer profile and the predicted numerical profile is higher, a little over 10%. The experimental thermal profile is cooler than expected compared to surface temperature as measured by pyrometry. The surface temperature extrapolated from interferometry in

Fig. 3 is 1007 K, which is 8.8% less than the surface temperature measured by the pyrometer.

These results demonstrate that interferometry is useful for investigating the thermal boundary layer prior to ignition. Even better comparison between experimental results and numerical predictions using a similarity solution was achieved when the vessel was filled with nitrogen gas rather than the hexane-air mixture reported here. From this, we conclude that mixtures containing hexane (and other fuels) are more difficult to process successfully with interferometry because of decomposition prior to a main ignition event [14, 12, 15]. Despite this challenge, interferometry processing of hexane mixtures was still reasonably successful. Experimental techniques measuring cylinder surface temperature agreed within 10% of each other, and the experimental results matched simple numerical predictions of the boundary layer within approximately 12% difference.

4. Experimental Results

Experiments are performed to investigate the effects of cylinder geometry and fuel choice. The ignition events are represented as a binary outcome variable where 0 represents no ignition, and 1 represents an ignition event. At least twenty individual experiments are performed for each condition in order to analyze the ignition data via logistic regression [16, 17, 18], to determine the probability of ignition as a function of cylinder surface temperature. The ignition thresholds we report are the temperature at which there is a 50% probability of ignition.

4.1. Study of Cylinder Size

For the study of cylinder size, each cylinder is tested in a stoichiometric n-hexane-air mixture at 101.3 KPa. Hexane is chosen as a fuel because it is a simple surrogate for aviation kerosene, widely used in explosive atmosphere tests and previous laboratory studies. The focus of the present work was on ignition behavior as function of surface area and height at fixed composition for the four fuels we tested.

Boeck et al. [19] made an extensive study of ignition temperature on a much smaller scale version of the current experiments and demonstrated a weak dependence of ignition temperature of n-hexane mixtures on composition away from the flammability limits. Martin and Shepherd [20] observed the same insensitivity to

composition for larger surface areas in AIT testing. Menon et al. [15] found that the insensitivity of the threshold to mixture composition is due to the important role that third body reactions play in the chain branching reaction at intermediate temperatures. As a consequence, the expectation is that pressure will be a more important factor than composition. From these considerations, we anticipate that mixture composition (away from the flammability limits) will have a modest effect on ignition thresholds and investigate only stoichiometric mixtures at atmospheric pressure in this work, while acknowledging that the effect of composition and pressure should be examined in future large scale testing.

4.1.1. Ignition Testing Results

Figure 5 shows an example of the logistic regression analysis performed on the results of testing cylinder 50A. The ignition threshold is 1078 K, and the confidence limits on the threshold, ±6 K are obtained from the 95% confidence limits determined by the logistic regression. This analysis is repeated on the ignition data for all cylinders except 25A, which failed due to buckling from thermal stress after five experiments. The ignition results and confidence limits are reported in Table 2. The ignition threshold reported for 25A is the lowest temperature at which an ignition event was observed for that cylinder.

Cylinder Tag	Ignition Temperature (K)	95% Confidence Limit (K)
25A	1113*	N/A
50A	1085	± 8
50C	1117	-
75B	1078	± 6
100A	1055	± 6
100C	1074	± 5
200A	1019	± 5

Table 2: Ignition temperatures and confidence limits for all cylinders. * indicates that the ignition temperature for 25A is the lowest ignition temperature observed in five experiments, rather than extracted from logistic regression.

We plot the ignition thresholds against surface area in Fig. 6. The ignition temperature gradually decreases as surface area increases, from 1113K at 25 cm^2 to 1019 K at 200 cm^2. This amounts to a total decrease in the ignition temperature of approximately 100 K (less than 10%) over a near order of magnitude change in

the surface area.

We also consider the effect of cylinder height on ignition threshold. Figure 6 shows that a change in height at a fixed surface area causes a relatively small change in the ignition temperature, indicating that the ignition temperature has a very modest dependence on the vertical extent. We further discuss the role of cylinder height in determining ignition temperature and flow regime in Section 5.

4.1.2. Comparison with Literature Data

Comparisons can also be made with literature results on thermal ignition by internal and external natural convection flows. Previous researchers often only report the minimum temperature at which ignition is obtained for a given configuration; these are the values given in the following discussion. For external natural convection, Melguizo-Gavilanes et al. [21] report ignition temperatures of n-hexane mixtures at 1275 ± 45 K for a glowplug with 1.5 cm^2 surface area. Boeck et al. [9] report ignition temperatures of 1270 K for a vertical cylinder 3.14 cm^2 in area. Ono et al. [7] report an ignition temperature of approximately 1250K for vertical plates 9 cm^2 in area in a propane-air mixture.

For internal natural convection flows, Kuchta et al. [2] studied ignition inside vessels of various shapes with surface areas larger than 40 cm^2. Kuchta et al. [2] found ignition temperatures of from 898 K at 40.5 cm^2 to 533 K at 171 cm^2 for hexane-air mixtures. White [22] studied ignition of kerosene-air mixtures inside vessels with 250 cm^2 or larger surface area, and found an ignition temperature of 530 K for the 250 cm^2 vessel. Boettcher [4] studied ignition of hexane inside a vessel 380 cm^2 in area, and found an ignition temperature of 473 K. Martin and Shepherd [5] reproduced the autoignition testing procedure prescribed by ASTM E659 [23] with spherical vessels 300 cm^2 in area, and found an ignition temperature of 508 K for hexane-air mixtures.

Figure 7 compares the data from all cited studies against results from this work. Two conclusions are drawn from this comparison. Ignition temperatures for external natural convection are consistently much higher than ignition temperatures for internal natural convection flows. Additionally, there is a significant difference in the trend of ignition temperature with surface area when comparing internal and external flows. Kuchta et al. [2] report ignition temperature dropping from 898 K at 40.5 cm^2 to 533 K at 171 cm^2 which amounts to a 365 K decrease in ignition

temperature over 130 cm^2 of area change. For a similar area change, the ignition temperature of the cylinders drops from 1117 K at 50 cm^2 to 1019 K at 200 cm^2. This is a difference of 98 K over a 150 cm^2 area change. The precipitous drop in ignition temperature at around 75 cm^2 that Kuchta et al. [2] observed does not occur. Instead, there is only a slight and gradual decrease in the ignition temperature with increasing surface area for the external flows. This indicates that a change from internal to external flow has much more impact on ignition temperature than a change in surface area for the range investigated here.

4.1.3. Visualization Studies

Visualization of the ignition event also provides useful information about the ignition process. Visual observation of the ignition event reveals that the ignition kernel is consistently found to form at the top edge of the high-temperature portion of the cylinder. This is an expected result for the tests performed in this work, which are designed to identify the ignition threshold. Trying to find the ignition threshold (minimum ignition temperature) means ignition occurs at the location where a fluid particle has been exposed to elevated surface temperatures the longest. For the vertical cylinders, this location is at the top edge of the high temperature region.

Figure 8 provides a few representative sequences of ignition on cylinder 100C using interferometry, dot schlieren (also called dark-field schlieren, see [24]) imaging, and OH* chemiluminescence to visualize the ignition event. Column (a) uses interferometry, column (b) uses dot schlieren imaging, and column (c) uses OH* chemiluminescence for visualization. The surface temperature at ignition was 1093 for (a), 1080 for (b), and 1090 K for (c). Frames are compared at similar times relative to ignition across all three visualization techniques. Ignition is considered to be the point at which the flame is first visible outside of the cylinder surface, as the cylinder itself blocks any information about the flame before it propagates outside the edges of the cylinder for interferometry and schlieren imaging.

The flame is observed to propagate in a general "barrel" shape in all three visualization techniques, as the flame propagates faster in the vertical direction than the horizontal direction. Observation of the flame propagation reveals that the flame travels up and down the cylinder at an average speed of 6.4 m/s, while in the horizontal direction it travels at an average speed of 3.0 m/s. The reason for the difference in flame speed between the horizontal and vertical directions is attributed to the temperature difference between the heated thermal layer and

the cool ambient mixture. The flame propagates faster in the vertical direction, where it remains near the heated surface in the high temperature thermal boundary layer, than in the horizontal direction, where it propagates into the cool ambient conditions.

The flame speed, V_s, can be estimated from the computed laminar burning speed, S_L and σ, the ratio of the unburned to burned gas density:

$$V_s = S_L \sigma = S_L \frac{\rho_u}{\rho_b} . \tag{2}$$

The values computed from this expression are only intended to be order of magnitude estimates due to lack of complete symmetry in flame shape, nonuniform temperature, and flow induced by flame propagation. The laminar burning speed and expansion ratio are computed using Cantera [25]. The variation of observed flame speed with location in the thermal layer can be explained by the dependence of flame speed on unburned gas temperature. The ratio of the laminar burning speed between any two temperatures scales as approximately the square of the temperature ratio [26, 27, 28]. The expansion ratio scales with the inverse of the temperature ratio so that the flame speed scales approximately linearly with temperature. Calculations with the hexane mechanism presented in Coronel et al. [29] predict a flame speed of 3.1 m/s at a temperature of 300 K. This matches the horizontal flame speed observed in the experiments of 3.0 m/s. The calculations also predict a flame speed of 6.4 m/s at a temperature of 700 K, which matches the film temperature of the experimental boundary layer. This flame speed matches the observed vertical flame speed of 6.4 m/s.

4.2. Study of Jet A and Surrogates

Experiments are performed with Jet A and surrogate fuel mixtures. We test a blend of Jet A, POSF-4658, whose composition has been thoroughly characterized [30], as well as two multicomponent surrogate fuels, JI [31] and Aachen [32]. Martin and Shepherd [5] investigated these fuels in the context of the ASTM autoignition tests [23], and identified these two fuels as generally suitable surrogates for POSF-4658 Jet A in the low pressure and temperature regime of autoignition. Table 3 lists the composition of the multicomponent fuels.

The multicomponent fuels Aachen and JI require higher ambient temperature conditions in order to achieve full vaporization [33], which is necessary for precise

		% by Weight		
		Aachen	JI	POSF-4658
H/C ratio		2.016	2.019	1.935
Avg. Molecular Formula		$C_{9.77}H_{19.7}$	$C_{12.49}H_{25.22}$	$C_{11.69}H_{22.62}$
Alkanes	n-Alkanes	80	29.17	19
	iso-Alkanes	-	46.53	31.34
	cyclo-Alkanes	-	-	28.42
	Total	80	75.7	78.76
Aromatics	Alkylbenzenes	20	4.94	13.69
	Alkylnapthalenes	-	-	1.76
	Cycloaromatics	-	19.41	5.79
	Total	20	24.35	21.24

Table 3: Comparison of composition of jet fuel blend and surrogate fuels

control of the mixture composition. Control of the POSF-4658 Jet A mixture composition is achieved in a slightly different manner, but is still ultimately controlled via ambient temperature. Therefore, in order to create Jet A and surrogate fuel mixtures with well-controlled mixture compositions, it is necessary to heat the entire experimental setup to temperatures as high as 400 K.

The fuels were tested at vessel temperatures corresponding to the temperature needed to fully vaporize the fuel (for surrogates JI and Aachen) or to create the desired mixture composition (for POSF-4658 Jet A). Sund [33] calculates a dew temperature of 333 K for Aachen. Preliminary vaporization tests for Aachen were performed with the vessel temperature at 333 K, and partial pressure measurements indicated that the fuel had not fully vaporized; the pressure dropped several torr after the initial injection of the fuel and the measured pressure of the fuel vapor was less than half of the expected fuel vapor for the given fuel sample. Vaporization tests with Aachen at a vessel temperature of 373 K indicated that the fuel had fully vaporized. A similar approach was taken with JI: full vaporization was not achieved at the predicted dew temperature of 373 K. Vaporization tests at 393 K indicated full vaporization of the sample of JI.

In contrast to the surrogate fuels, due to the presence of high molecular weight species, it is not possible to fully vaporize Jet A at the maximum operating tem-

perature of our apparatus. Instead, we inject a known quantity of Jet A into the vessel to create a layer of liquid fuel at the bottom and allow the liquid and vapor to come to equilibrium. The preferential vaporization of lighter components and depletion from the liquid will result in the vapor phase fuel composition being different from the liquid, which can be accounted for as described by Sund [33]. This method has the advantage of simplicity and reproducability. Previous studies have shown that a lower fuel mass loading (the ratio of fuel mass to vessel volume) results in a lower total vapor pressure of the fuel [34, 35]. Shepherd et al. [35] find that with a lower fuel mass loading (3 vs 400 kg/m^3) not only is the fuel vapor pressure lower, but the relative amount of lower molecular weight fuels is decreased as well as lower molecular weight components are depleted from the liquid fuel due to vaporization. Large fuel mass loadings provide enough of a liquid fuel reservoir within the combustion vessel to minimize depletion of light species. However, Shepherd et al. [36] found a limited influence of the fuel mass loading between 3 and 400 kg/m^3 on the ignition energy in electrical spark ignition testing. We assume a similar limited influence of fuel mass loading on thermal ignition threshold and in order to keep the experimental procedure manageable, we investigate Jet A ignition using a fuel mass loading of 3 kg/m^3. This amounts to 150 mL of fuel added to the vessel for each experiment.

The vapor pressure of Jet A is controlled via the temperature of the vessel. Shepherd et al. [37] measured the vapor pressure as a function of vessel temperature and developed correlation for jet fuels over a range of flash point temperatures. From these correlations, we predict a vessel temperature of 333 K will create the Jet A fuel vapor pressure needed for a stoichiometric fuel-air mixture, and vaporization tests confirmed a temperature of 333 K was sufficient for achieving the desired Jet A vapor partial pressure.

Hexane fully vaporizes at the room temperature so the vapor composition is never in question. Limited testing was carried out with hexane at a vessel temperature of 393 K to match the highest vessel temperature used in Jet A and surrogate experiments and to examine the effect of increased ambient temperature on ignition thresholds. All fuels were tested in a stoichiometric fuel-air mixture (equivalence ratio of 1.0), except for JI, which was tested at an equivalence ratio of 0.75.

4.2.1. Ignition Data from Fuel Tests

All experiments investigating fuel choice are performed with cylinder 200A. At least twenty individual tests are performed for each fuel, and an ignition threshold is extracted for each fuel using a logistic regression analysis as previously described. The ignition results are tabulated in Table 4.

Fuel	Vessel Temp. (K)	Ign. Temp. (K)	Conf. Limits (K)
Hexane (ambient temp)	295	1019	± 5
Hexane (high temp)	393	933	± 12
Aachen	373	948	± 12
JI	393	984	± 3
Jet A (POSF-4658)	333	971	± 7

Table 4: Vessel temperature, ignition temperature, and confidence limits for all surrogate testing as well as regular and high ambient temperature testing of hexane.

The JI ignition temperature is 13 K (1.3%) higher than the POSF-4658 Jet A ignition temperature, while the ignition temperature of Aachen is 23 K (2.4%) lower than that of POSF-4658 Jet A. The high ambient temperature hexane tests had an ignition temperature 38 K (3.9%) lower than POSF-4658 Jet A, while the room temperature hexane tests had an ignition temperature 48 K (4.9%) higher than POSF-4658 Jet A.

The difference in ignition temperatures between hexane and POSF-4658 Jet A is less than 5% but larger than the 50°F (28 K) difference required by the FAA between reported literature autoignition temperatures of Jet A and maximum allowable temperatures in a flammable leakage zone [1]. Hexane is often used in explosive atmosphere testing as a surrogate for Jet A due to its simplicity (vaporizes at room temperature, single-component fuel) but if the minor differences in ignition temperature are of concern, the JI surrogate appears to be a more appropriate alternative.

4.2.2. Effect of Ambient Temperature

We can investigate the effect of ambient temperature on ignition threshold by comparing the results of testing cylinder 200A with hexane at an ambient temperature of 293 K (from Section 4.1) with the results of hexane at an ambient temperature of 393 K. At 293 K with cylinder 200A, hexane ignited at 1019 K. At

393 K with cylinder 200A, hexane ignited at 933 K. This amounts to a decrease in ignition threshold of 86 K for a 100 K increase in ambient temperature. This difference is significantly larger than the estimated uncertainty in the ignition temperature measurement and we conclude that increasing the ambient temperature causes a decrease in ignition threshold.

There are a few studies reporting the effects of increased ambient temperature on thermal ignition. Mullen et al. [38] investigated thermal ignition by horizontal rods under forced convection and saw a slight decrease in ignition temperature with an increase in ambient temperature. The effect became more pronounced at higher flow velocities: a 5 K decrease in ignition temperature occurs at a flow rate of 24.4 m/s, and an 89 K decrease in ignition temperature occurs at a flow rate of 48.8 m/s when the ambient temperature is increased by 61 K. Ono et al. [7] examined the effects of surface size on thermal ignition by vertical plates in free convection. They also noted a decrease in the ignition temperature as the ambient temperature was increased: the ignition temperature dropped by approximately 20 K with a 40 K increase in the ambient temperature. Ono et al. noted that for a given wall temperature, an increased ambient temperature reduces the convection velocity of natural convection flows, and cited the reduced velocity (leading to a longer time for the mixture to pass through the boundary layer) as the cause for a reduced ignition temperature.

We can investigate this claim by using a similarity solution to model the development of a natural convection boundary layer (see Section 4 of the Supplementary Materials). We investigate the effects of a change in the ambient temperature. First, we calculate the similarity solution with a wall temperature of 1100 K, and change the ambient temperature from 300 to 400 K. With an ambient temperature of 300K, the maximum velocity in the momentum boundary layer is 1.52 m/s. With an increased ambient temperature of 400 K, the maximum velocity in the momentum boundary layer is 1.22 m/s. We see exactly the sort of decrease in convection velocity that Ono et al. cite in their study of effects of ambient temperature on ignition.

We can also think of the change in ignition temperature with increased ambient temperature in terms of the Van't Hoff ignition criterion, which states that ignition occurs when the thermal gradient at the surface is zero. The Van't Hoff criterion can be represented as:

$$\left(\frac{dT}{dy}\right)_w = 0\,. \tag{3}$$

The Van't Hoff criterion implies that heat loss at the surface is balanced by heat transfer due to chemical reactions [39]. It is apparent that for the same wall temperature, an increase in the ambient temperature produces a significantly shallower thermal gradient in the thermal layer. A shallower thermal gradient in the thermal boundary layer implies it will take less additional energy by chemical reaction to reach the Van't Hoff criterion, and therefore makes ignition possible at lower surface temperatures when the ambient temperature is increased.

Similarity solution estimates of the boundary layer profile for the room-temperature hexane tests and the high temperature hexane tests are presented in Fig. 9. We see that the higher ambient temperature condition indeed has a significantly shallower thermal gradient in the boundary layer profile.

5. Discussion

While results in the previous sections are reported in terms of surface area in order to enable comparison with historical data, there is no compelling scientific basis to expect a significant correlation of ignition results with surface area. A more rational basis for the correlation of ignition temperature with source size can be found in studies that have applied the classical Frank-Kamenetskii theory of thermal explosions to natural convection. Ono et al. [7] proposes a correlation of ignition temperature with the height of the vertical surface based on work by Khitrin and Goldenberg [40], and Laurendeau [39] extends this discussion to a variety of situations and discusses the flow scaling in terms of the Grashof or Rayleigh number and the parameters of one-step chemical reaction models.

Ono et al. [7] proposes that for free convection flows, $\ln(L^{1/2}) \propto \frac{E_a}{RT_{ign}}$; L is characteristic surface height for the case of natural convection, E_a is activation energy, R is the universal gas constant, and T_{ign} is the ignition temperature. This can be rearranged to indicate the scaling of ignition temperature with characteristic size of the surface: $T_{ign} \propto \frac{2E_a}{R\ln(L)}$, which can be generalized to be a nondimensional correlation of the form,

$$\frac{L}{L^*} = f\left(\frac{E_a}{RT_{ign}}, Gr, \ldots\right)\,, \tag{4}$$

where L^* is a reference length and there may be additional non-dimensional parameters to account for geometric factors and properties of the combustible gas. The scaling of ignition temperature with height proposed by Ono et al. [7] is supported by theoretical analyses and numerical simulations [39, 41].

For vertical natural convection flows, there is no obvious choice for L^* from the geometry. Possibilites include a reference flame thickness or the boundary layer thickness at some reference location. Lacking a sufficient range of data to test these choices, we follow the empirical approach of Ono et al. [7] to correlate the present ignition data using the cylinder height for the length L. For a given geometry, initial pressure, and fuel type, Ono et al. [7] demonstrate that experimental data on ignition temperature and surface height are well correlated by,

$$\ln(L) = \frac{C_1}{T_{ign}} + C_2 \ , \tag{5}$$

or

$$T_{ign} = \frac{C_1}{\ln(L) - C_2} \ , \tag{6}$$

C_1 and C_2 are empirical constants determined from fitting the experimental data. Ono et al. [7] demonstrates the validity of this correlation on vertical heated plates with $0.5 < L < 3$ cm. The present data extends the range of L up to 25 cm for vertical heated cylinders.

The comparison of Eq. 6 with the data from this work is shown in Fig. 10. Although the data is very sparse, the trend is reasonable and predicts that for laminar flow, continuing to increase the cylinder height will result in further decreases in T_{ign}, below 900 K for $L = 1000$ cm. All of these results are in the laminar flow regime $Gr \leq 10^7$. The Grashof numbers of the cylinders investigated in this study range from $5.3 \times 10^6 < Gr < 4.2 \times 10^7$, and transition to turbulence is estimated to occur around $Gr \approx 10^8$, so these cylinders are approaching transitional flow. In contrast to the very modest decrease in ignition temperature with increasing height, the Grashof number will increase as the cube of characteristic length, $Gr = \frac{g\beta(T_{ign}-T_\infty)L^3}{\nu^2}$ or $Gr \propto L^3$. As shown on the plot, the dramatic increase in Gr with increasing height is predicted to result in transition to turbulence, which will likely have a significant impact on the ignition temperature and an altogether different scaling relationship than for laminar flow.

The physical-chemical explanation of boundary layer ignition dependence on scale is subtle. Gas that enters the boundary layer near the bottom of the vertical cylinder remains near the surface for a very long time due to the no-slip condition at the surface and is hot enough to react. However, the energy released by the combustion processes is primarily transferred back into the surface rather than outward into the adjacent gas in the boundary layer. So those gas elements right at the surface are not responsible directly for ignition but do provide a source of reactive species.

Gas elements on streamlines entering the boundary layer at higher elevations convect upward and toward the surface, gaining thermal energy and reactive species by diffusion from gas closer to the wall and losing it to gas further out. Gas that is too far from the wall will never get sufficiently hot or gain enough reactive species to ignite and remain unreacted until reached by the flame propagating from the ignition kernel.

Ignition takes place on a streamline that is near but not too near the wall and the ignition event occurs when the balance between energy gain by chemical reaction exceeds the energy loss to both the hot surface and fluid in the outer portions of the boundary layer. Diffusion of radical species and reactive intermediates from the near wall region outward to the ignition location also plays a significant role in the ignition process. The location of the ignition onset is too close the cylinder surface to be observed with our instrumentation but is predicted by simulations [12, 14, 15] to be on the order of magnitude of the flame thickness. The critical balance required for ignition can be achieved at a lower temperature if the magnitude of the surface normal temperature gradient is lower at the point of ignition, reducing the rate of thermal transport away from the ignition location. From the scaling of solutions to the boundary layer equations, we find that increasing the cylinder height decreases the magnitude of temperature gradient at the top of the cylinder as the boundary layer thickness δ increases with cylinder height H as $\delta \propto H^{1/4}$ Decreasing the cylinder temperature will also decrease the magnitude of the temperature gradient proportionately.

Ignition processes are often analyzed conceptually in terms of a critical ratio (Damköhler number) between a flow time scale, often expressed as a residence time, and a reaction time scale which is usually taken to be inversely proportional to the reaction rate. However, there is not a single well-defined residence time or reaction rate for natural or forced convection boundary layers. There is a range of

values of residence time from infinity at the hot surface to zero for gas beyond the outer edge of the boundary layer. More importantly, the temperature and velocity histories are distinct for each streamline (examples are given in the Supplementary Material) and cannot be characterized by residence time alone. The lack of a well-defined residence time is one of the essential differences between ignition in a recirculating flow and a boundary layer.

6. Conclusions

An extensive series of tests demonstrated that over the range of parameters examined, surface area and length of the cylinder have a minor effect on ignition temperature. In contrast to the results found by Kuchta et al. [2] for internal natural convection flows, no drastic change of the ignition temperature was observed for the vertical cylinders with surface areas between 25 and 200 cm^2. Additionally, the ignition threshold of the external natural convection flows was 500-600 K higher than ignition thresholds of internal natural convection flows with the same surface area. The ignition data fit well with the logarithmic scaling of ignition temperature with height first proposed by Ono et al. [7].

Investigation of fuel choice showed that hexane is a reasonable surrogate for POSF-4658 Jet A in external natural convection ignition tests. JI, a multicomponent surrogate, has an ignition threshold closest to POSF-4658 Jet A of all the fuels tested (13 K difference in ignition thresholds). All the fuels investigated had ignition temperatures differing from that of POSF-4658 Jet A by 38 K or less.

This study has significant implications for safety assessments involving hot surface ignition. The present results make it clear that the purported correlation of ignition temperature with surface area presented by Kuchta et al. [2] is actually a consequence of changing the geometry of the test from unconfined external convection to a confined, internal convection flow. This indicates a need to focus attention on the fluid mechanics, extent of confinement, and the distinction between internal (recirculating) flows and external (free convection) flows rather than surface area alone. In the case of laminar external natural convection, the present study demonstrates that significantly (200-500 K) higher surface temperatures (on surfaces up to 200 cm^2 in area) may be present without causing ignition in flammable atmospheres containing Jet A or surrogate fuels. For engineering

applications with turbulent flow, further investigation is needed.

Funding: This work was supported by The Boeing Company through a Strategic Research and Development Relationship Agreement CT-BA-GTA-1.

References

[1] Federal Aviation Administration, Advisory circular 25.981-1D, 2018.

[2] J. Kuchta, A. Bartkowiak, M. Zabetakis, Hot surface ignition temperatures of hydrocarbon fuel vapor-air mixtures, J. Chem. Eng. Data 10 (1965) 282–288.

[3] F. White, Heat Transfer, Addison-Wesley, 1984.

[4] P. Boettcher, Thermal Ignition, Ph.D. thesis, California Institute of Technology, 2012.

[5] C. Martin, J. Shepherd, Low Temperature Autoignition of Jet A and Surrogate Jet Fuels, 13th International Symposium on Hazards, Prevention, and Mitigation of Industrial Explosions, 2020. Paper No. 973.

[6] G. Adomeit, Ignition of gases at hot surfaces under nonsteady-state conditions, Symp. (Int.) Combust. 10 (1965) 237–243.

[7] S. Ono, H. Kawano, H. Niho, G. Fukuyama, Ignition in a Free Convection from Vertical Hot Plate, Bull. JSME 19 (1976) 676–683.

[8] J. Melguizo-Gavilanes, A. Nové-Josserand, S. Coronel, R. Mével, J. E. Shepherd, Hot Surface Ignition of *n* -Hexane Mixtures Using Simplified Kinetics, Combust. Sci. Tech. 188 (2016) 2060–2076.

[9] L. R. Boeck, M. Meijers, A. Kink, R. Mével, J. E. Shepherd, Ignition of fuel–air mixtures from a hot circular cylinder, Combust. Flame 185 (2017) 265–277.

[10] L. Michalski, K. Eckersdorf, J. Kucharski, J. McGhee, Temperature Measurement, John Wiley & Sons, 2001.

[11] W. Merzkirch, Flow Visualization, Academic Press, 1987.

[12] S. A. Coronel, J. Melguizo-Gavilanes, R. Mével, J. E. Shepherd, Experimental and numerical study on moving hot particle ignition, Combust. Flame 192 (2018) 495–506.

[13] L. R. Cairnie, A. J. Harrison, Natural Convection Adjacent to a Vertical Isothermal Hot Plate with a High Surface to Ambient Temperature Difference, Int. J. Heat Mass Transf. 25 (1982) 925–934.

[14] S. A. Coronel, Thermal Ignition Using Moving Hot Particles, Ph.D. thesis, California Institute of Technology, 2016.

[15] S. K. Menon, P. A. Boettcher, B. Ventura, G. Blanquart, Hot surface ignition of n-hexane in air, Combust. Flame 163 (2016) 42–53.

[16] S. Bane, J. Shepherd, E. Kwon, A. Day, Statistical analysis of electrostatic spark ignition of lean H_2/O_2/Ar mixtures., Int. J. Hydrog. Energy 36 (2011) 2344–2350.

[17] D. Hosmer, S. Lemeshow, R. Sturdivant, Applied Logistic Regression, John Wiley & Sons, 1989.

[18] J. Neter, M. H. Kutner, W. Wasserman, C. J. Nachtsheim, Applied Linear Statistics Models, McGraw Hill, 1996.

[19] L. Boeck, M. Meijers, A. Kink, R. Mével, J. E. Shepherd, Ignition of fuel-air mixtures from a hot circular cylinder, Combust. Flame 185 (2017) 265–277.

[20] C. Martin, J. Shepherd, Autoignition testing of hydrocarbon fuels using the ASTM-E659 method., Technical Report EDL2019.002, Graduate Aeronautical Laboratories, California Institute of Technology, 2019.

[21] J. Melguizo-Gavilanes, A. Nove-Josserand, S. Coronel, R. Mevel, J. E. Shepherd, Hot surface ignition of n-hexane mixtures using simplified kinetics, Combust. Sci. Tech. 188 (2016) 2060–2076.

[22] R. White, Spontaneous Ignition of kerosene (AVTUR) Vapour: the effect of the ratio, vessel surface area to volume, Technical Report 67107, Royal Aircraft Establishment, 1967.

[23] ASTM International, ASTM E659-15, Standard Test Method for Autoignition Temperature of Chemicals, 2015.

[24] G. S. Settles, Schlieren and Shadowgraph Techniques, Springer Berlin Heidelberg, first edition, 2001.

[25] D. G. Goodwin, R. L. Speth, H. K. Moffat, B. W. Weber, Cantera: An object-oriented software toolkit for chemical kinetics, thermodynamics, and transport processes, 2018. Version 2.4.0, https://www.cantera.org.

[26] G. L. Dugger, D. D. Graab, Flame velocities of hydrocarbon-oxygen-nitrogen mixtures, Symp. (Int.) Combust. 4 (1953) 302 – 310.

[27] A. G. Gaydon, H. G. Wolfhard, Flames; their structure, radiation and temperature, Chapman and Hall, London, UK, 1960.

[28] A. Konnov, R. Meuwissen, L. de Goey, The temperature dependence of the laminar burning velocity of ethanol flames, Proc. Combust. Inst. 33 (2011) 1011–1019.

[29] S. Coronel, J. Melguizo-Gavilanes, D. Davidenko, R. Mével, J. E. Shepherd, Reduction methodology for detailed kinetic mechanisms: Application to n-hexane-air hot surface ignition, 2017. 11th Asia-Pacific Conference on Combustion, The University of Sydney, NSW Australia, 10-14 December 2017.

[30] J. T. Edwards, Reference Jet Fuels for Combustion Testing, 55th AIAA Aerospace Sciences Meeting, 2017. No. 2017-0146.

[31] X. Chen, E. Khani, C. Chen, A unified jet fuel surrogate for droplet evaporation and ignition., Fuel 182 (2016) 284—-291.

[32] S. Honnet, K. Seshadri, U. Niemann, N. Peters, A surrogate fuel for kerosene, Proc. Combust. Inst. 32 (2009) 485—492.

[33] S. M. Sund, Thermal Ignition of Surrogate Jet Fuels, Master's thesis, University of South-Eastern Norway, 2019.

[34] J. Lee, J. Shepherd, Spark Ignition Measurements in Jet A: part II, Technical Report FM99-7, California Institute of Technology, 2000.

[35] J. E. Shepherd, C. D. Nuyt, J. L. Lee, Flash Point and Chemical Composition of Aviation Kerosene (Jet A), Technical Report FM99-4, California Institute of Technology, 2000.

[36] J. Shepherd, J. Krok, J. Lee, Spark Ignition Energy Measurements in Jet A, Technical Report FM97-9, California Institute of Technology, 1999.

[37] J. Shepherd, J. Krok, J. Lee, Jet A Explosion Experiments: Laboratory Testing, Technical Report FM97-5, California Institute of Technology, 1997.

[38] J. W. Mullen, J. B. Fenn, M. R. Irby, The ignition of high velocity streams of combustible gases by heated cylindrical rods, Symposium on Combust. Flame, and Explosion Phenomena 3 (1948) 317–329.

[39] N. M. Laurendeau, Thermal ignition of methane-air mixtures by hot surfaces: A critical examination, Combust. Flame 46 (1982) 29–49.

[40] L. Khitrin, S. Goldenberg, The influence of the initial temperature of a combustible mixture and of the ambient pressure on the stabilization limits, Symp. (Int.) Combust. 6 (1957) 448 – 451.

[41] L. Chen, G. Faeth, Ignition of a combustible gas near heated vertical surfaces, Combust. Flame 42 (1981) 77 – 92.

[42] W. Navidi, Statistics for Engineers and Scientists, McGraw-Hill Higher Education, 2007.

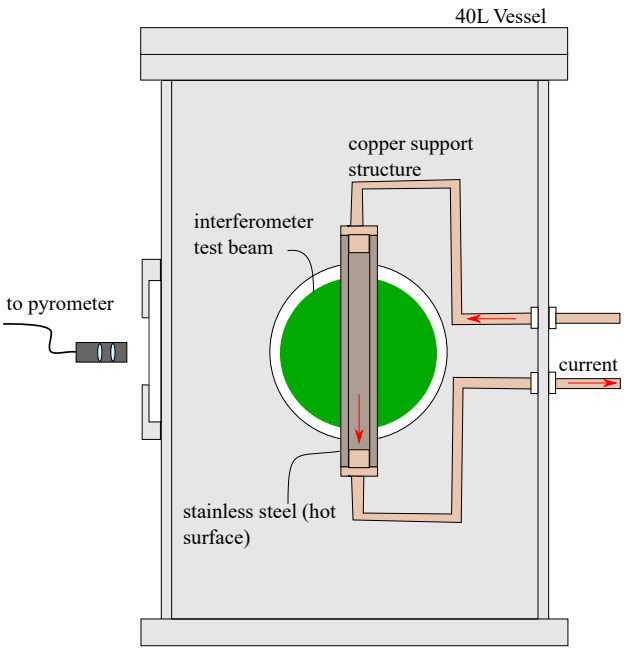

Figure 1: Schematic of Experimental Setup.

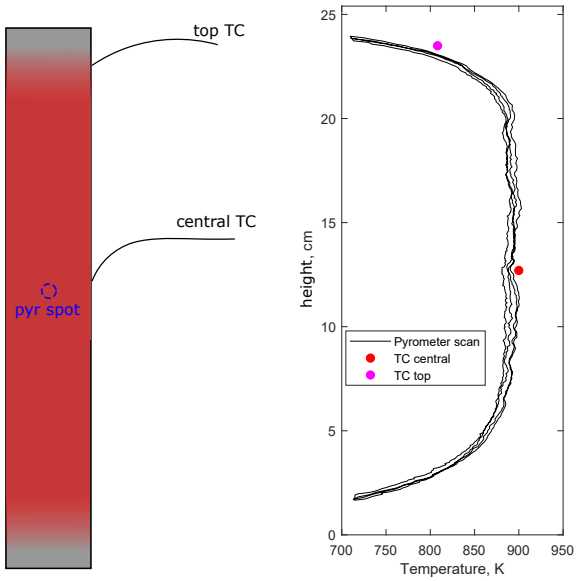

Figure 2: (Left) Schematic of thermocouples and pyrometer during heating tests. The central hot region is indicated in red, fading to the cooler edge region in gray. (Right) Temperature distribution along cylinder height from pyrometer characterization compared with thermocouple measurements.

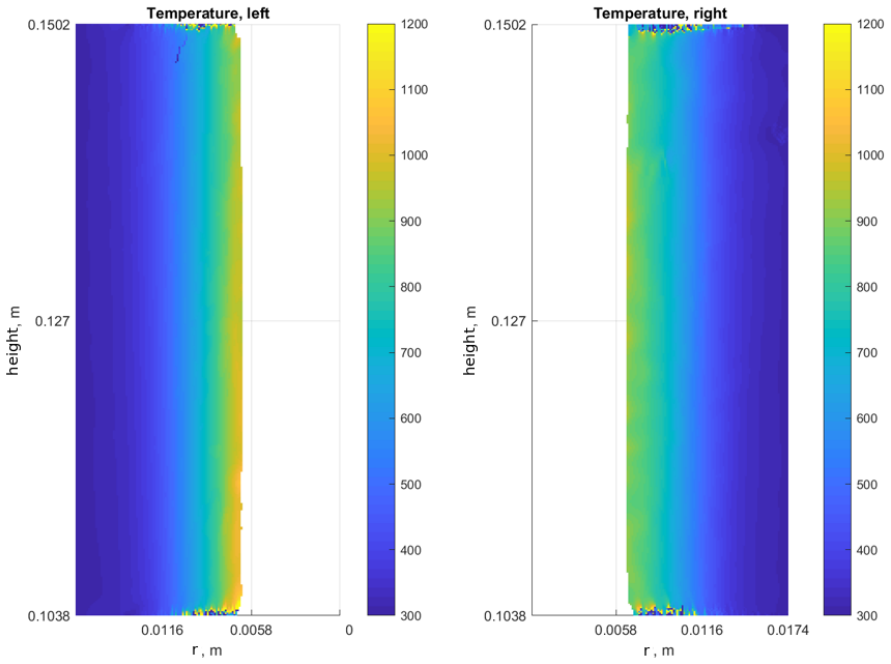

Figure 3: Temperature fields from interferometry for hexane test. Surface temperature measured by pyrometer = 1104 K.

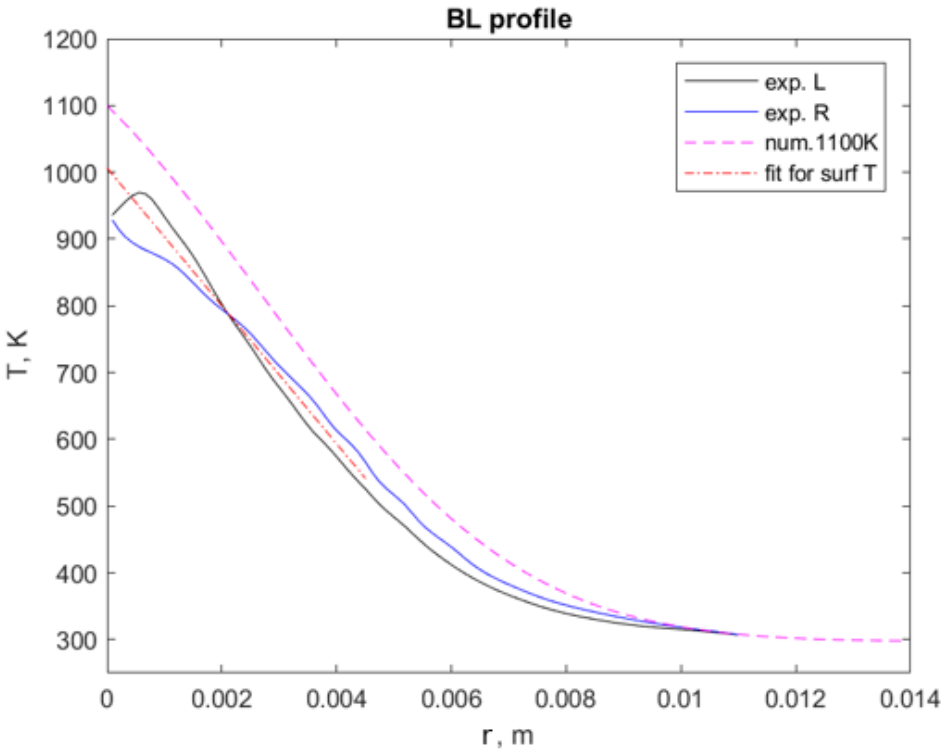

Figure 4: Thermal boundary layer profiles for left (black line) and right (blue line) sides of experimental results compared with prediction of boundary layer profile (dashed magenta line) based on similarity solution for pyrometer surface temperature. Linear fit to averaged experimental profile (red dot-dashed line) used to extrapolate surface temperature from interferometer post processing. Extrapolated interferometer surface temperature = 1006.5 K.

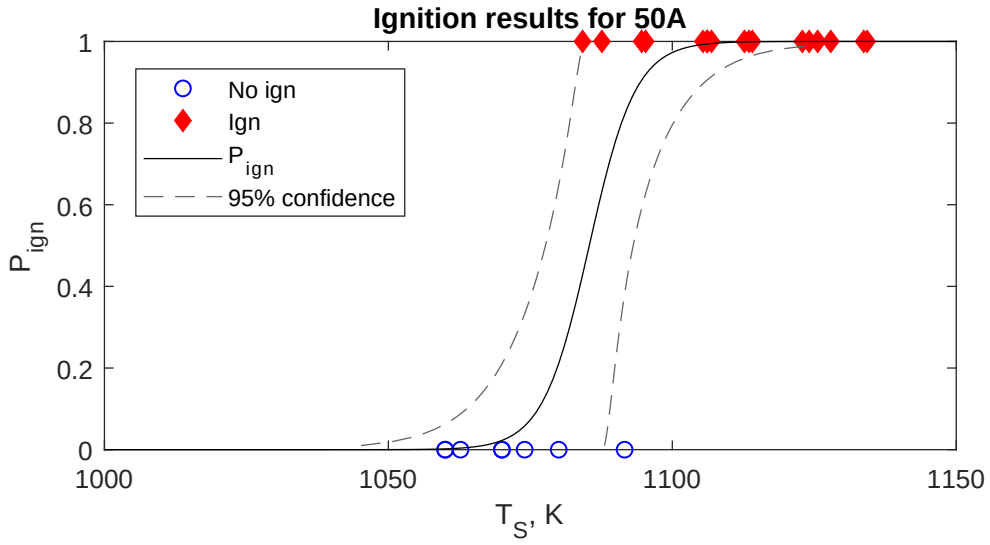

Figure 5: Ignition data for cylinder 50A. Test results show overlap in temperatures for ignition (red filled diamonds) and non-ignition (empty blue circles) results. The black line shows the probability of ignition as a function of temperature and the gray dashed lines show the 95% confidence limits on the probability function where applicable.

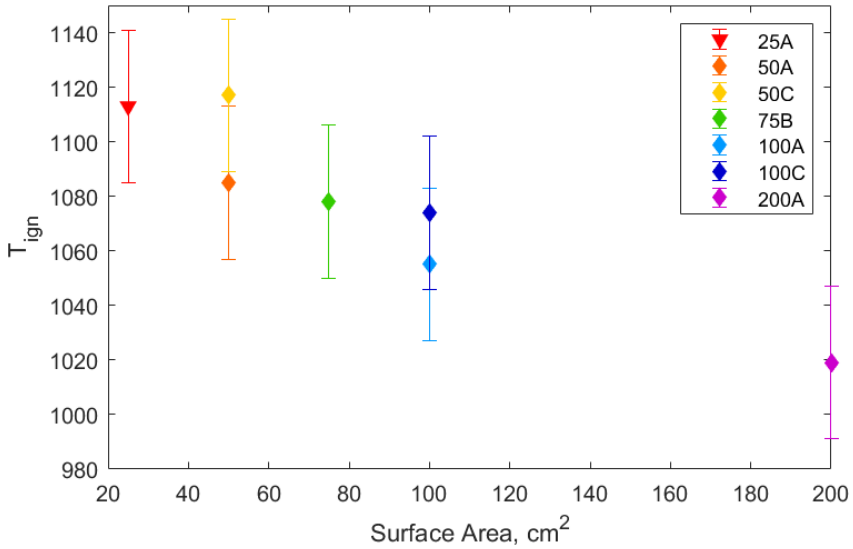

Figure 6: Plot of T_{ign} vs surface area for all cylinders. Error bars represent measurement uncertainty for pyrometer.

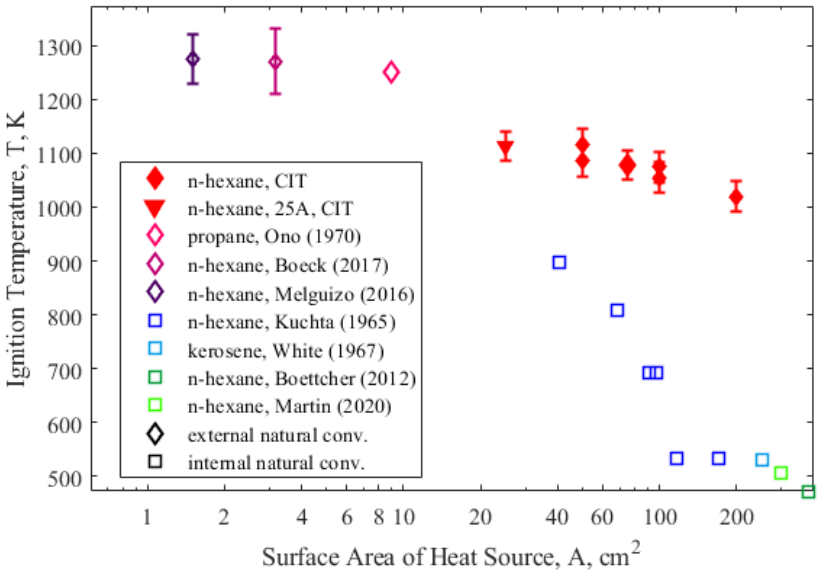

Figure 7: T_{ign} versus surface area for all vertical cylinder data points (red-filled markers. Red-filled diamonds for ignition temperatures extracted from full logistic regression, red-filled triangles for ignition temperature from lowest ignition of 25A) compared with wider literature on thermal ignition. Empty diamonds represent literature on thermal ignition by external natural convection, empty squares represent literature on thermal ignition by internal natural convection.

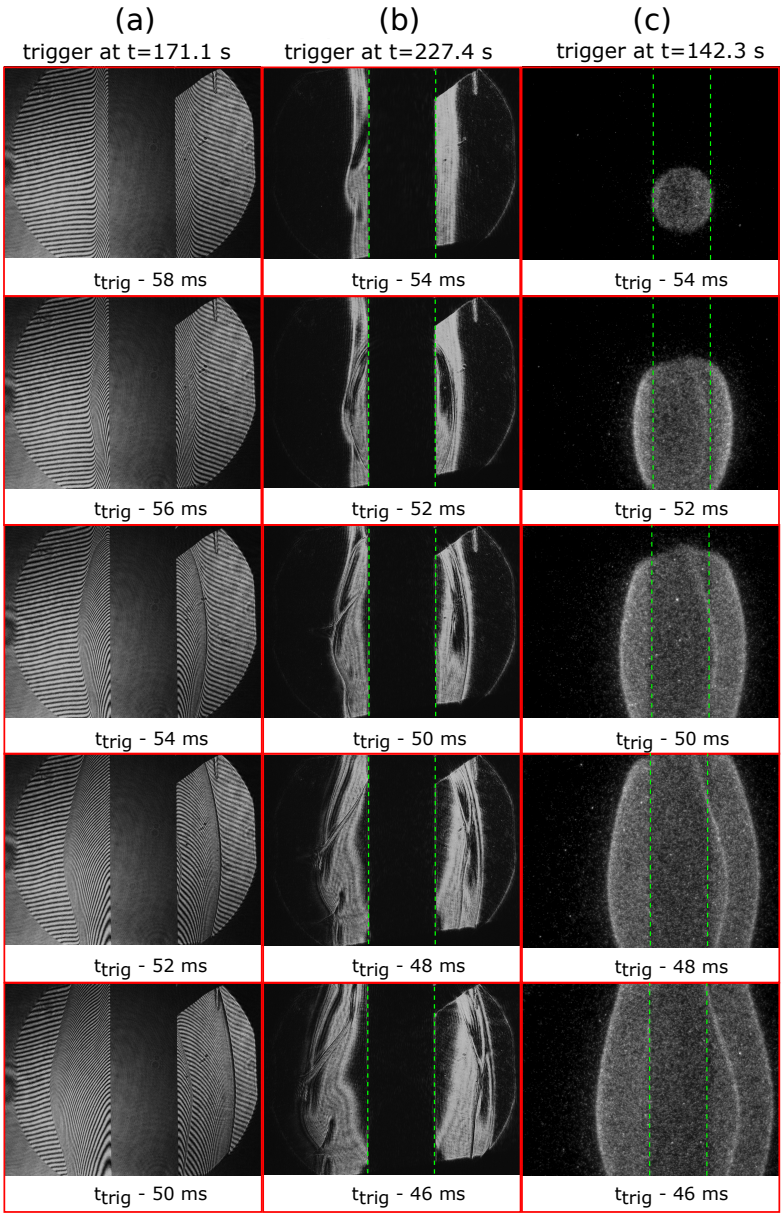

Figure 8: Side-by-side visualization of ignition from cylinder 100C testing. Column (a) uses interferometry, column (b) schlieren imaging, and column (c) OH* chemiluminescence. Time given relative to trigger for each frame in units of miliseconds. Visualization over the first 10 ms after ignition, defined here as the first sign of ignition appearing past the surface the cylinder. Ignition occurred at surface temperatures of 1093, 1080, and 1090 K, respectively.

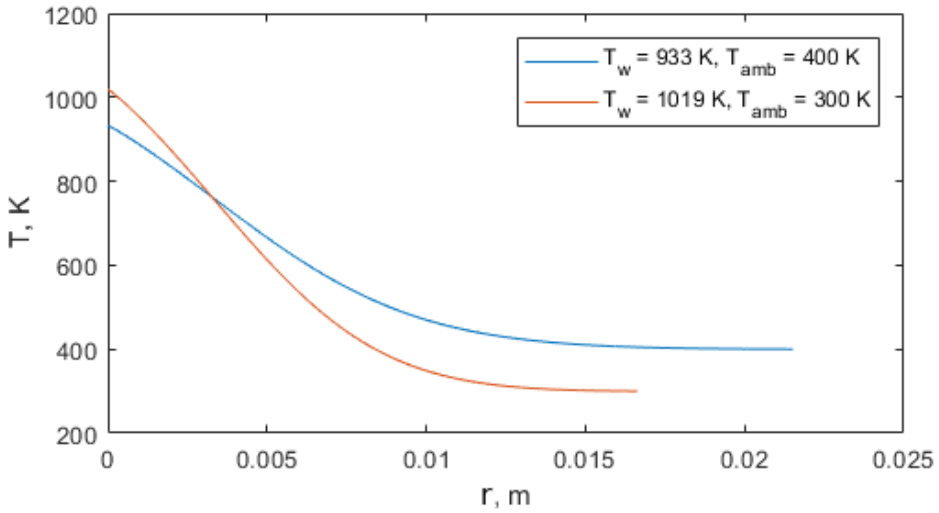

Figure 9: Effect of ambient temperature on boundary layer profiles as calculated via similarity solution using ignition temperatures from hexane testing as wall temperatures.

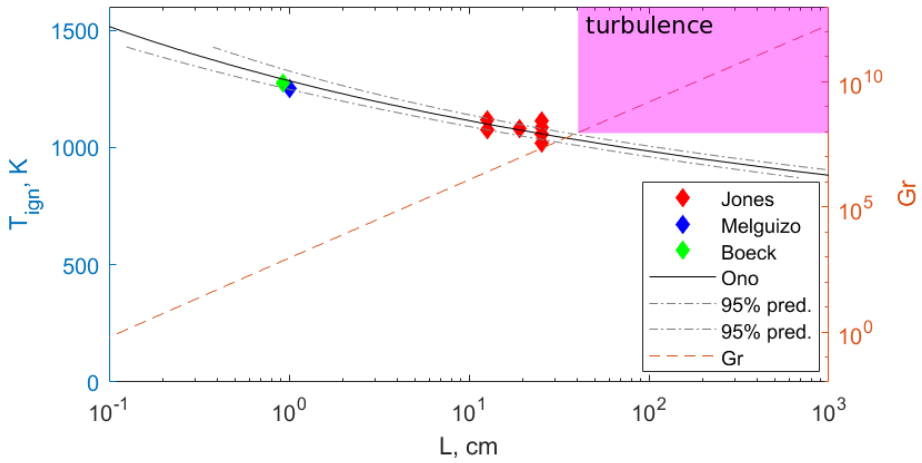

Figure 10: Comparison of data from this work and other Caltech data [8, 9] with Ono correlation: $\ln(L) = C_1/T_{ign} + C_2$. Through a linear regression analysis of the data, we find $C_1 = 19381 \pm 2869$ K, $C_2 = -15.09 \pm 2.58$. Note C_1 is reasonably consistent with the value of $E_a/R = 20740$ K predicted independently from analysis of a detailed hexane mechanism by Boeck et al. [9]. The gray dot-dashed lines represent the 95% prediction limits (uncertainty associated with using this correlation to predict future measurements). Details on the linear regression analysis are given in Navidi [42].

Thermal Ignition by Vertical Cylinders: Supplementary Materials

Silken Jones, Joseph Shepherd

California Institute of Technology,
1200 E. California Blvd., Pasadena, California, 91125, United States

1. Vessel Heating Setup

Experiments with heavier multicomponent fuels require heating of the entire experimental setup. A multi-zone heating system is installed, with a total available power of 10.8 kW, which is subdivided into six zones that can be separately powered and controlled, each with a power of 1.8 kW per zone. Each zone has a number of flexible silicone-rubber heaters from Omega and a type E thermocouple for temperature monitoring. The heaters are arranged into zones such that there is a compromise between an even power split between zones and keeping all heaters in a zone relatively close to one another to enable accurate temperature monitoring by thermocouple. Closed-loop control of temperature is achieved with Watlow 935A PID controllers. This ensures the temperature is relatively uniform across the vessel (within approximately $\pm$ 5 K). This, combined with the mixing of the gas inside the vessel before the experiments, ensures a uniform temperature in the flammable mixture at the start of the experiment.

Thermal insulation blankets were installed around the vessel to minimize heat loss. The heating system was able to raise the temperature of the experimental setup to over 400 K. The full details of the heating setup can be found in Jones [1].

Email address: smjones@caltech.edu (Silken Jones)

2. Cylinder Heating Temperature History

Figure 2 shows an example of a typical temperature history during heating of a cylinder. The surface temperature of the cylinder is monitored by a thermocouple (placed above the point where ignition occurs so that the presence of the thermocouple does not disturb or alter the thermal boundary layer in that region) and by a two-color pyrometer. The surface temperature of the cylinder is fed back to a LabView script that provides closed-loop control on the surface temperature. When the temperature of the cylinder is within five percent of the set steady-state temperature in LabView, the control loop kicks in and drives the temperature to the set value. Note that the pyrometer reading is noisy at the start of the heating process due to a small signal-to-noise ratio from minimal light emission at the two pyrometer-measured wavelengths when the surface temperature is low.

3. Interferometer Validation

The interferometer is validated by investigating the temperature fields it captures from heating a well-characterized surface (Autolite glowplug from Boettcher [2], Melguizo-Gavilanes et al. [3]). The glowplug is placed in the vessel in the interferometer field of view (Fig. 3). The vessel is filled with nitrogen and the glowplug is heated while its temperature is monitored by a type K thermocouple and by pyrometry. Interferometer images are captured and post processed as described by Coronel et al. [4]. The temperature fields from interferometry are compared to a simulation from Melguizo-Gavilanes et al. [3], shown in Fig. 4. The interferometer temperature fields compare well with previous numerical results, with less than 10% error everywhere except right along the centerline above the glowplug as shown in Figures 5 and 6. A narrow region of higher error occurs along the centerline due to the nature of Nestor-Olsen algorithm, which converts line of sight integrated quantities into radial quantities by working from the outside of the image in towards the centerline. This causes a buildup of errors along the centerline of the processed image. This validation demonstrates the accuracy of the interferometer in extracting quantitative gas temperature fields surrounding heated surfaces. Details of the optical engineering and design can be found in Jones [1].

4. Natural Convection Boundary Layer Model

A similarity solution is used to model the the steady boundary layer created by the natural convection flow induced by the hot cylinder. The goal of this part of the study was to explore the features of the steady boundary layer prior to ignition so the gas is modeled as inert air and no chemical reactions are considered. The temperature difference between the wall and the ambient gas is large enough that gas properties are considered a function of temperature. In order to take advantage of prior work on the similarity solution approach, a Cartesian geometry is considered, i.e., the hot surface is approximated as a vertical plate. This is a reasonable assumption as long as the boundary layer is sufficiently thin compared to the cylinder radius [5]. This is validated by comparison of interferometry results and computed boundary layer temperature profiles as discussed in Section 3 of the article. The following section describes the similarity solution used to develop a prediction for boundary layers in a natural convection flow with variable properties.

The analysis of the boundary layer is based on the low-speed, variable-density, two-dimensional steady boundary layer equations (1)-(3). Following the analysis of Sparrow and Gregg [6], we make the assumptions of constant pressure, variable density flow, an ideal gas, and neglect pressure work and viscous dissipation.

$$\frac{\partial(\rho u)}{\partial x} + \frac{\partial(\rho v)}{\partial y} = 0\,, \tag{1}$$

$$\rho\left(u\frac{\partial u}{\partial x} + v\frac{\partial u}{\partial y}\right) = g(\rho_\infty - \rho) + \frac{\partial}{\partial y}\left(\mu\frac{\partial u}{\partial y}\right)\,, \tag{2}$$

$$\rho c_p\left(u\frac{\partial T}{\partial x} + v\frac{\partial T}{\partial y}\right) = \frac{\partial}{\partial y}\left(\lambda\frac{\partial T}{\partial y}\right)\,. \tag{3}$$

The approach by Sparrow and Gregg [6] uses a stream function, ψ, that accounted for the variable density character of the flow. The equation for conservation of mass is automatically satisfied by using ψ, and the momentum and energy equations replace u and v with derivatives of ψ

$$u = \frac{\rho_r}{\rho}\frac{\partial\psi}{\partial y}\,, \qquad v = -\frac{\rho_r}{\rho}\frac{\partial\psi}{\partial x}\,, \tag{4}$$

This yields a set of coupled, two-dimensional partial differential equations for ψ and T as functions of x and y. Instead, we opt to transform the momentum and energy equations into ordinary differential equations through a transformation to a single independent similarity variable η.

$$\eta = \frac{c}{x^{\frac{1}{4}}} \int_0^y \frac{\rho}{\rho_r} dy,\; c = \left[\frac{g(\rho_\infty - \rho_r)/\rho_r}{4\nu_r^2} \right]^{\frac{1}{4}}, \tag{5}$$

where the reference condition r is selected to be the value at the hot surface, denoted w for wall. This transformation is motivated by the Howarth-Dorodnitsyn approach to compressible flow. This is analogous to the traditional similarity approach used for natural convection flows that are treated with the Boussinesq approach and constant fluid properties [7]. Transformed dependent variables are:

$$F(\eta) = \left(\frac{\psi}{x^{\frac{3}{4}}} \right) \left(\frac{1}{4\nu_r c} \right),\; \theta = \frac{T - T_\infty}{T_w - T_\infty}\,. \tag{6}$$

The perfect gas and constant pressure assumptions can be used to simplify the dimensionless buoyancy force:

$$\frac{(\rho_\infty/\rho) - 1}{(\rho_\infty/\rho_w) - 1} = \frac{T - T_\infty}{T_w - T_\infty} = \theta\,. \tag{7}$$

The momentum and energy equations are transformed into ordinary differential equations where F and θ are functions of η alone:

$$\frac{\partial}{\partial \eta} \left[\frac{\rho\mu}{\rho_r \mu_r} F'' \right] + 3FF'' - 2(F')^2 + \theta = 0\,, \tag{8}$$

$$\frac{\partial}{\partial \eta} \left[\frac{\rho\lambda}{\rho_r \lambda_r} \theta' \right] + 3Pr_r \left[\frac{cp}{cp_r} \right] F\theta' = 0\,, \tag{9}$$

with isothermal boundary conditions at the boundaries and a no-slip condition at the hot surface.

$$F(0) = F'(0) = 0, \theta(0) = 1, F'(\infty) = \theta(\infty) = 0\,. \tag{10}$$

Following the analysis laid out by Cairnie et al. [8], we assume the combination of fluid properties that appear as coefficients vary with temperature as follows:

$$M(\theta) = \frac{\rho\mu}{\rho_r \mu_r}\,, \tag{11}$$

$$\dot{M}(\theta) = \frac{dM}{d\theta}\,, \tag{12}$$

$$L(\theta) = \frac{1}{Pr_r}\left(\frac{c_{p_r}}{c_p}\right)\frac{\rho\lambda}{\rho_r\lambda_r}\,, \tag{13}$$

$$Y(\theta) = \frac{1}{Pr_r}\left(\frac{c_{p_r}}{c_p}\right)\frac{d}{d\theta}\left(\frac{\rho\lambda}{\rho_r\lambda_r}\right)\,. \tag{14}$$

The functions M, $\dot{M}$, L, and Y were represented as fits to tabulated properties of high-temperature air. Using the defined property functions, the final form of the similarity version of the boundary layer equations is:

$$MF''' + \dot{M}\theta' F'' + 3FF'' - 2(F')^2 + \theta = 0\,, \tag{15}$$

$$L\theta'' + Y(\theta')^2 + 3F\theta' = 0\,, \tag{16}$$

The functions F and θ are determined by numerical solution of the two-point boundary value problem (15) and (16) with boundary conditions (10) using MATLAB's `bvp4c` solver. Our solution is validated against the results presented by Cairnie and Harrison [8] and the details of the validation are presented in [1]. The results for u-velocity, v-velocity, and temperature are shown in Fig. 7.

The numerical results in Figure 7 are for a 25.4-cm-tall plate. Results for a shorter plate can be obtained by truncating the numerical results at the desired total height of the plate. Velocity fields parallel (u-velocity) and perpendicular (v-velocity) to the wall and temperature fields are presented. The wall parallel velocity takes the expected structure for a natural convection flow: no-slip creates a velocity of zero next to the wall. Buoyancy forces increase the velocity as distance from the wall increases, reaching a maximum before velocity drops again to zero at the edge of the momentum layer to match ambient conditions. Similarly, wall perpendicular velocity appears as expected for a natural convection flow. The velocity is largest and negative at the leading edge of the cylinder as gas is entrained into the natural convection flow. The entrainment effect becomes less pronounced along the outer edge of the momentum layer as distance from the leading edge increases. As expected, the perpendicular velocity next to the wall is zero. Temperature results show the gas matches wall temperature immediately next to the surface, and then gas temperature drops off rapidly until ambient temperature

is approached at the edge of the thermal layer. Additionally, the width of the momentum and thermal layers increase very quickly in approximately the first centimeter along the plate, after which there is a much more gradual increase in width as the distance from the leading edge increases.

4.1. Streamlines

The similarity approach described previously can be used to model streamlines of a natural convection flow. The stream function ψ is computed from:

$$\psi = 4\nu_w x^{3/4} \left(\frac{g(T_w - T_\infty)}{4\nu_w^2 T_w} \right)^{1/4} F(\eta) \,. \tag{17}$$

The similarity variable can be implicitly determined as a function $\eta(x, y)$ from (5) once the function $\theta(\eta)$ has been calculated. The stream function, ψ, is then normalized by the maximum value of the stream function in the domain:

$$\psi_n = \frac{\psi}{\psi_{max}} \,. \tag{18}$$

Streamline trajectories $x(y)$ are defined implicitly by solving (17) with a constant value of ψ. A wide range of ψ_n values were chosen to allow the selection of streamlines close to the hot surface as well as streamlines that barely enter the thermal layer. Nine values of the normalized stream function, ψ_n, were used to define the streamlines shown in Fig. 8. Once streamlines are selected, the (x, y) position, the wall parallel and perpendicular velocities u, v, and the temperature, T at every point along each streamline are saved and used to compute the temperature history.

The time history of the streamline is calculated by the following procedure: compute the arc length, s, along the streamline and integrate the reciprocal of arc velocity with respect to arc length. The change in arc length is defined as:

$$ds^2 = dx^2 + dy^2 \,, \tag{19}$$

and we define $s = 0$ at the start of the streamline such that all subsequent arc lengths can be found by:

$$s_i = s_{i-1} + \sqrt{dx_i^2 + dy_i^2} \,. \tag{20}$$

The total time to move along the streamline is given by:

$$t_s = \int_0^s \frac{1}{\sqrt{u^2 + v^2}} ds \,. \tag{21}$$

The velocities (u, v) are calculated from the stream function. The temperature histories of gas elements moving along selected streamlines are shown in Fig. 9.

We observe that once streamlines enter the boundary layer, the wall normal distance remains relatively constant over the height of the plate. In particular, fluid elements on the streamlines entering the boundary layer closest to the bottom travel nearly parallel to the plate and move very slowly in the very low-speed portion of the momentum boundary layer adjacent to the wall. These fluid elements also reach high temperatures rapidly as shown in Figure 9. We anticipate on the basis of the temperature history that chemical reaction will occur rapidly on those streamlines closest to the surface. However, most of the energy released in the reaction process will be absorbed by the nearby wall if it is highly conductive, as is the case for our metal cylinder. So it is not possible for an ignition event to happen for those streamlines which have the longest residence time at high temperatures.

Instead, ignition will take place slightly further away on streamlines that are close but not too close to the wall. Although the gas will heat more gradually and not get as hot as the surface, it will not lose as much heat to the surface. Streamlines that are far from the surface never get sufficiently hot to react before the top of the plate is reached.

We conclude that there is an optimal streamline and distance from the plate for ignition to occur. The temperature history is sufficient to initiate reaction before the top of the plate is reached and energy released by chemical reaction on this optimal streamlines can create a sufficiently hot spot to ignite a propagating flame in the surrounding gas.

However, it is very challenging to identify the streamline or location in the boundary layer from this heuristic analysis. A detailed simulation accounting not only for heat transfer but also chemical reaction and species transport is required.

References

[1] S. Jones, Thermal Ignition by Vertical Cylinders, Ph.D. thesis, California Institute of Technology, 2021. https://resolver.caltech.edu/CaltechTHESIS:12182020-055522985.

[2] P. Boettcher, Thermal Ignition, Ph.D. thesis, California Institute of Technology, 2012.

[3] J. Melguizo-Gavilanes, A. Nove-Josserand, S. Coronel, R. Mevel, J. E. Shepherd, Hot surface ignition of n-hexane mixtures using simplified kinetics, Combust. Sci. Tech. 188 (2016) 2060–2076.

[4] S. Coronel, J. Melguizo-Gavilanes, S. Jones, J. Shepherd, Temperature field measurements of thermal boundary layer and wake of moving hot spheres using interferometry, Experimental Fluid and Thermal Science 90 (2018) 76–83.

[5] E. M. Sparrow, J. L. Gregg, Laminar-Free-Convection Heat Transfer From the Outer Surface of a Vertical Circular Cylinder, Transactions of the ASME 78 (1956) 1823–1829.

[6] E. M. Sparrow, J. L. Gregg, The variable fluid property problem in free convection, Transactions of the ASME 80 (1958) 879–886.

[7] S. Ostrarch, An Analysis of Laminar Free Convection Flow and Heat Transfer About a Flat Plate Parallel to the Direction of the Generating Body Force, Technical Report NACA TR 1111, NASA, 1953.

[8] L. R. Cairnie, A. J. Harrison, Natural Convection Adjacent to a Vertical Isothermal Hot Plate with a High Surface to Ambient Temperature Difference, Int. J. Heat Mass Transf. 25 (1982) 925–934.

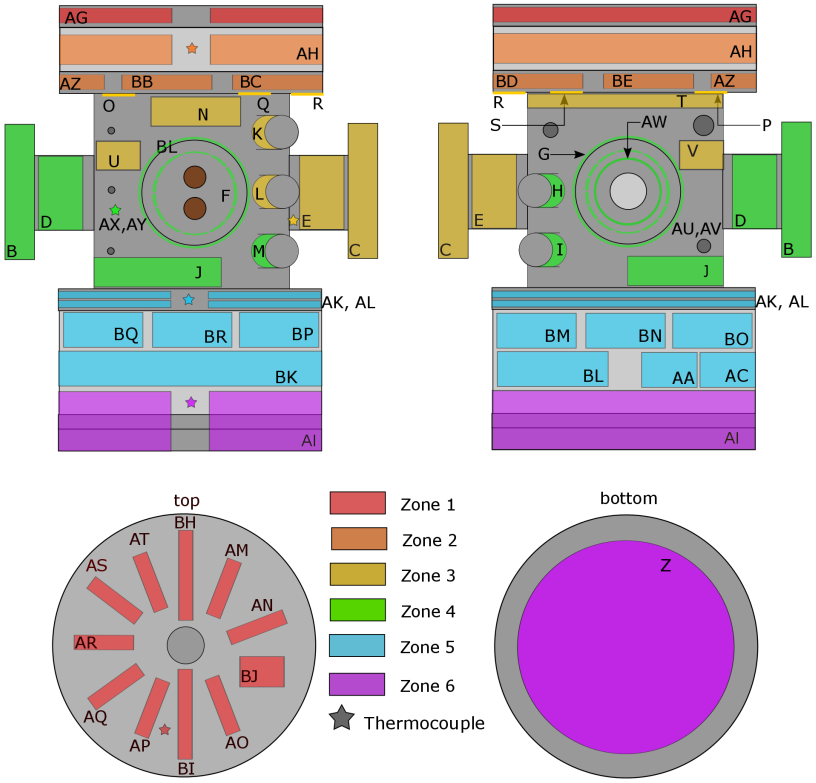

Figure 1: Zoned heating system for mutlicomponent fuel testing.

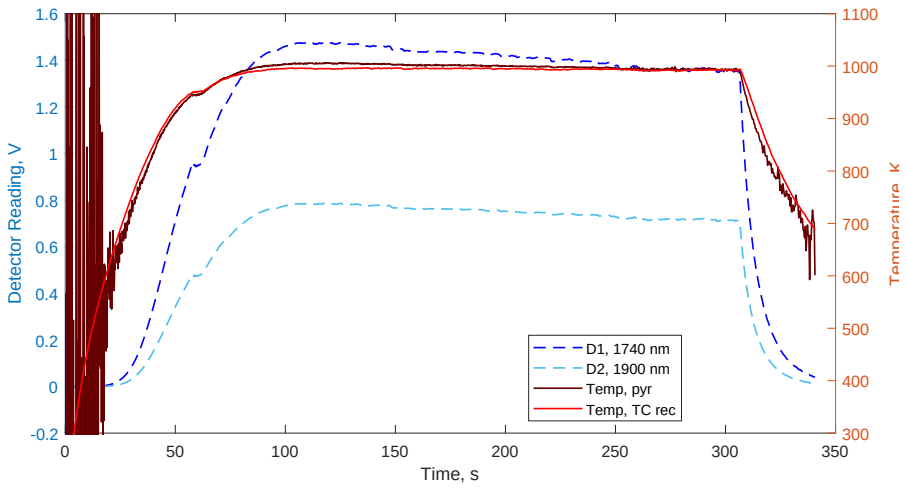

Figure 2: Temperature history of typical cylinder heating event. The dark red line represents the temperature from pyrometry and bright red line represents reconstructed temperature at the centerline as measured by the top thermocouple. The light and dark blue dashed lines represent the voltage readings of the two oyrometer photo detectors during the heating process.

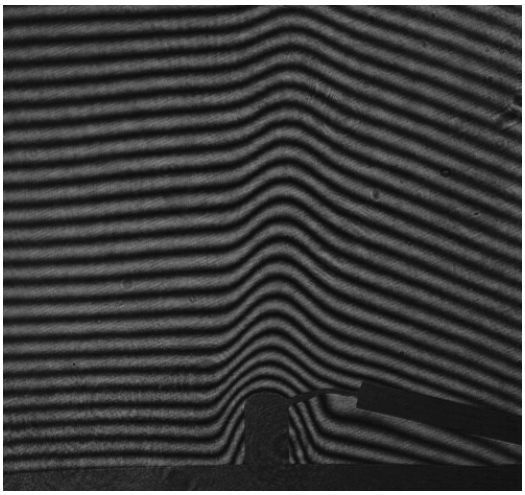

Figure 3: Raw interferogram of glowplug.

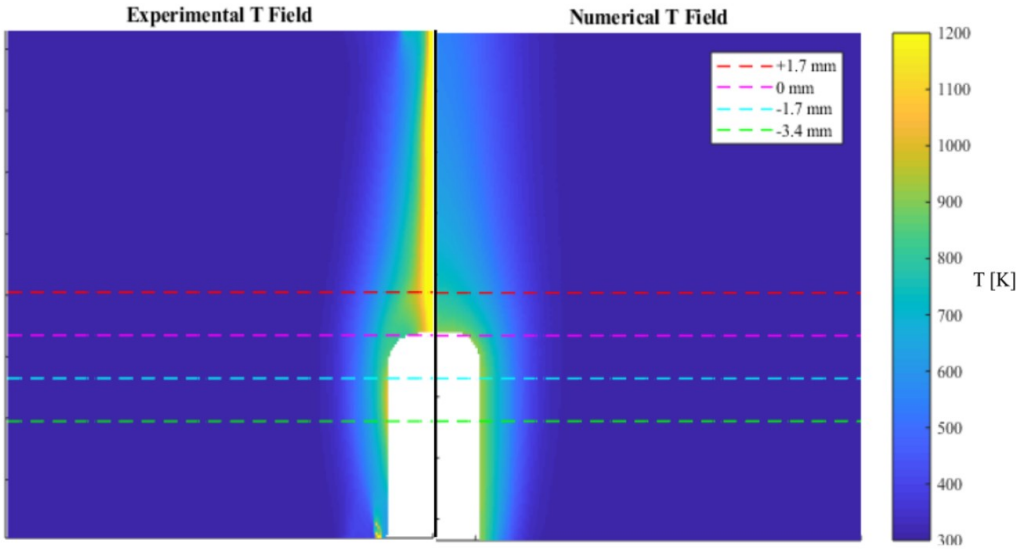

Figure 4: Temperature fields from interferometry (left) compared with simulations from Melguizo-Gavilanes et al. [3] (right).

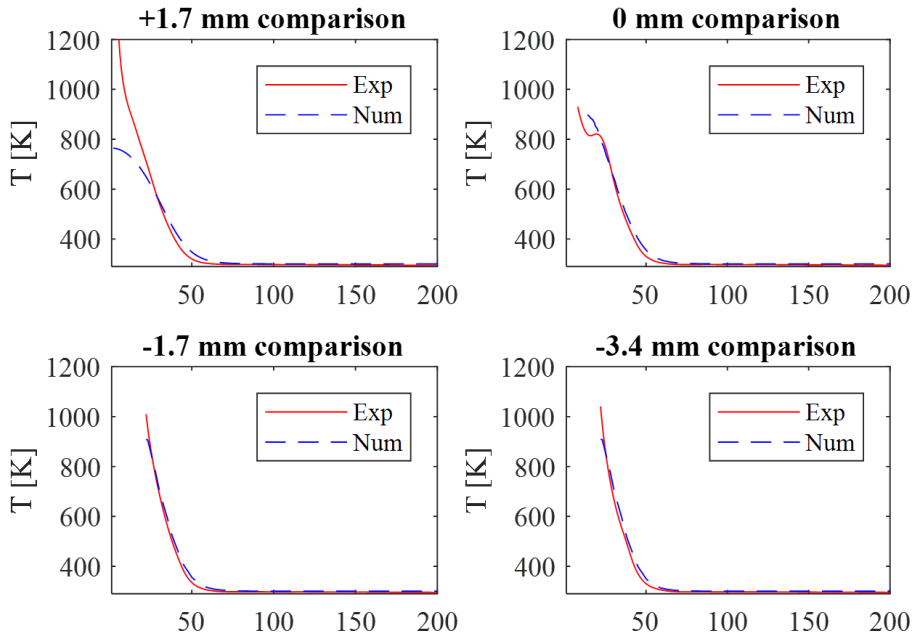

Figure 5: Thermal boundary layer profiles of experimental and numerical results compared for each of the four slices indicated in Figure 4. The labels on the abscissa are distance in pixels from the centerline (0.116 mm/px); each plot is labeled by the vertical distance above the top of the glow plug.

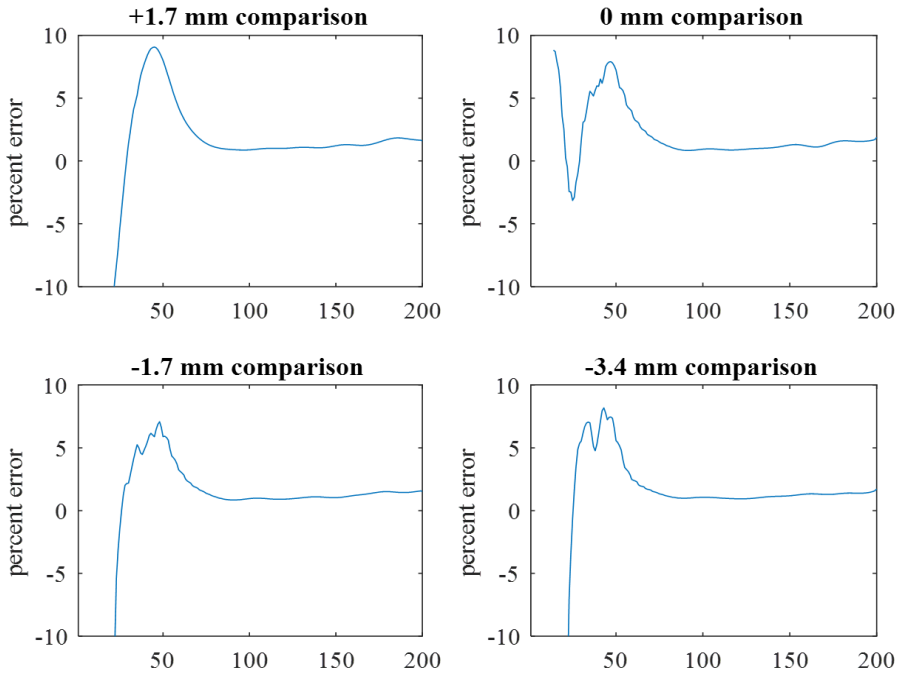

Figure 6: Percent error in thermal boundary layer between experimental and numerical results for each of the four slices as indicated in Figure 4. The labels on the abscissa are distance in pixels from the centerline (0.116 mm/px); each plot is labeled by the vertical distance above the top of the glow plug.

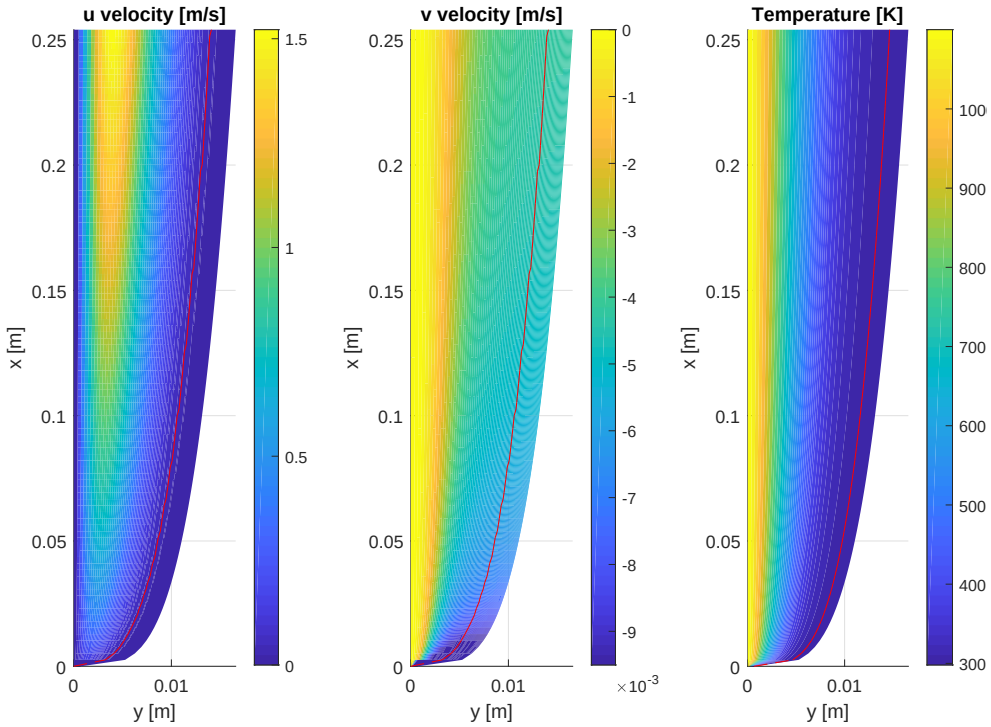

Figure 7: Results of similarity solution to thermal boundary layer on a vertical plate. Left: u-velocity field. Middle: v-velocity field. Right: temperature field. The wall temperature is 1100 K, the gas is dry air, and the plate is 25.4 cm long.

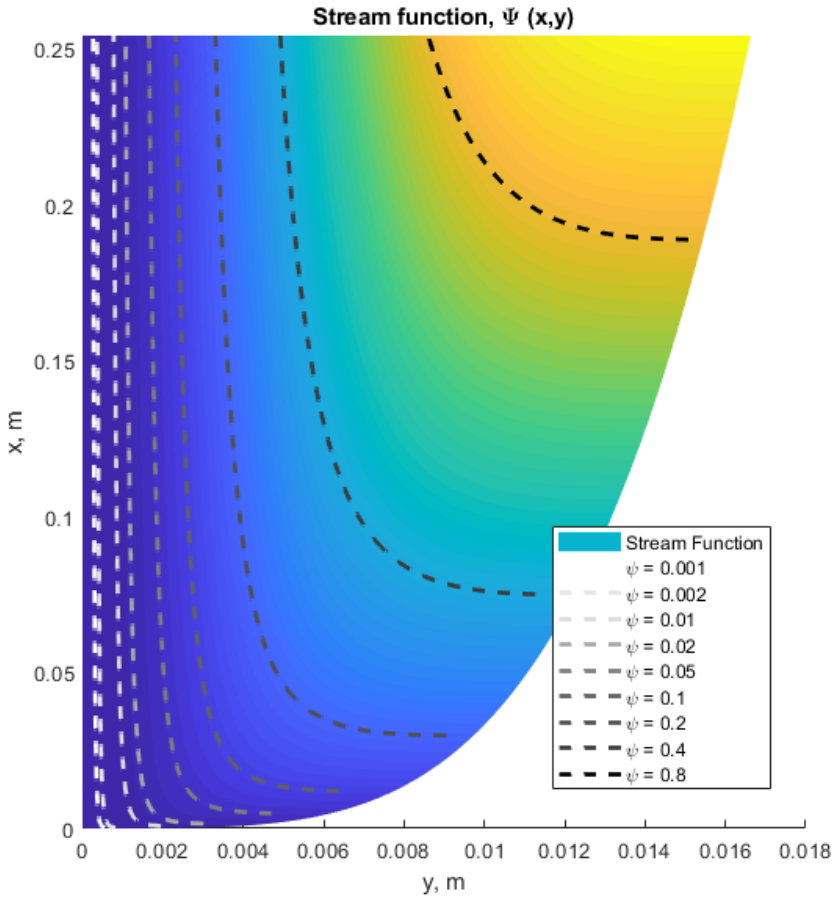

Figure 8: Normalized stream function, ψ_n, from similarity solutions. Selected streamlines for tracking highlighted with dashed gray lines.

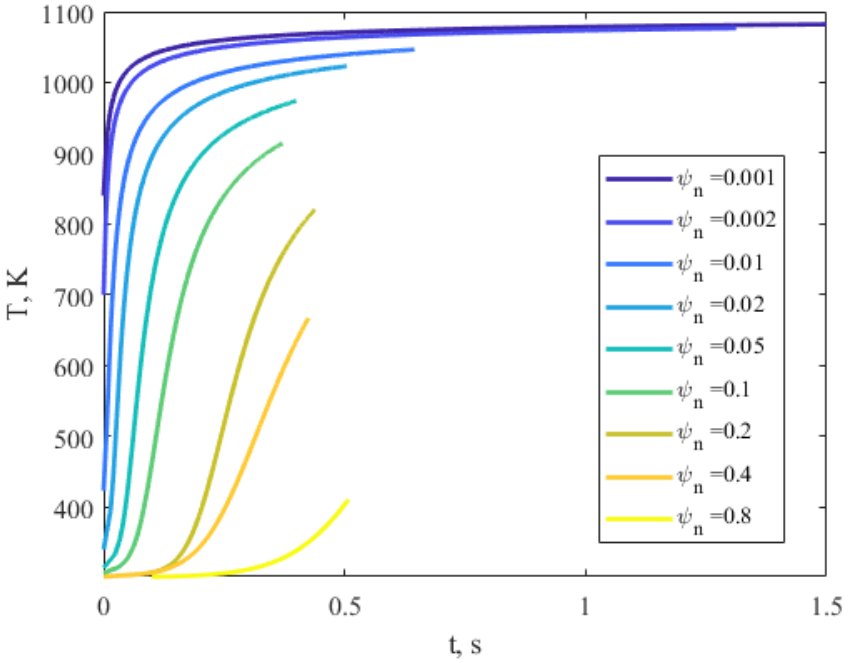

Figure 9: Stream function temperature history from similarity solutions.